ACS Photonics

Article

pubs.acs.org/journal/apchd5

Binary Additives Regulate the $PC_{71}BM$ Aggregate Morphology for Highly Efficient Polymer Solar Cells

Xi Fan,*[,†] Jinzhao Wang,[‡] Huihui Huang,[§] and Hao Wang*[,†]

[†]Hubei Collaborative Innovation Center for Advanced Organic Chemical Materials, Faculty of Physics and Electronic Science, Hubei University, Wuhan 430062, People's Republic of China

[‡]Department of Material Science and Engineering, Hubei University, Wuhan 430062, People's Republic of China

[§]College of Optoelectronic Engineering, Shenzhen University, Shenzhen 518060, People's Republic of China

ABSTRACT: We optimized the performance of polymer solar cells (PSCs) based on PBDTTT-C-T:$PC_{71}BM$ with the binary solvent additives of 1,8-diiodomethane (DIO) and chloronaphthalene (CN). The power conversion efficiency was significantly improved from 3.44% for the PSC without additives to 7.91% for the PSC with the additives (DIO/CN = 1:2). It is attributed to the achievement of highly penetrating $PC_{71}BM$ aggregate structures, which have small aggregate particles, and dense and well-packed pathways, inducing a high electron mobility. Our work not only provides an effective method to regulate the $PC_{71}BM$ aggregate structures for highly efficient PSC devices but also indicates an underlying mechanism of the performance enhancement by solvent additives.

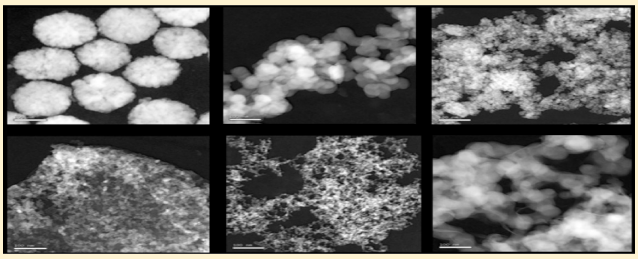

KEYWORDS: *morphology, $PC_{71}BM$ aggregate structures, binary additives*

Polymer solar cells (PSCs) are composed of a photoactive layer of conjugated polymer donor and fullerene derivative (typically PCBM or $PC_{71}BM$) acceptor sandwiched between a transparent indium tin oxide (ITO) anode and a low-work function cathode. The power conversion efficiency (PCE) of PSC devices is sensitive to the polymer/fullerene phase separation morphology in the active layers, because the polymer/fullerene interpenetrating networks in the active layer provide interfaces for exciton dissociation and charge-carrier transport pathway in PSC devices.[1−5] Therefore, recently, it has attracted much attention to improve photovoltaic performance of the PSC devices with every approach, including thermal annealing, solvent annealing, processing additive, and ring substituent on fullerene derivatives, to tune the phase separation morphology.[6−12] Among them, the processing additive is the most commonly used means of regulating the film morphology at present. However, it still remains challenging. On the one hand, a single additive is limited to control the PCBM (or $PC_{71}BM$) aggregate morphology and the degree of phase separation. When large-domain phase separation occurs, charge recombination will dominate in turn. On the other hand, there is a lack of direct evidence to give an insight into a distinct phase separation evolution, because atomic force microscopy is still a surface technology to characterize the morphology of thin films; whereas traditional transmission electron microscopy (TEM) measurement cannot distinctly demonstrate the information regarding the lateral phase segregated morphology of blend layers and $PC_{71}BM$ aggregate structures at present, especially in small dimension of below 20 nm, since the organic materials containing only light elements (such as C, H, N, O, and S) show poor contrast between the subphases in the TEM.[13,14] Therefore, both new additive recipes and effective characterization methods are urgent needs for the application of the PSC devices.

In this work, to enhance greatly the PSC device performance, and to correlate the photovoltaic performance with $PC_{71}BM$ aggregate structures, we first performed the optimization of the PSC devices based on PBDTTT-C-T:$PC_{71}BM$ with the five treatments of 3% 1,8-diiodomethane (DIO), 3% chloronaphthalene (CN), and the DIO/CN binary additives with a vol. ratio of 2:1% (2:1), 1.5:1.5% (1.5:1.5), and 1:2% (1:2), respectively. The PSC with the 1:2 binary additive treatment shows the best photovoltaic performance with a PCE of 7.91% and a short circuit current density (J_{SC}) of 16.81 mA cm^{-2}. Then, we introduced a novel characterization method to show the lateral morphology of $PC_{71}BM$ aggregate structures, which were achieved after washing out the polymer from the active layers by ultrasonic treatment. Since we focus our efforts on the characterization of the $PC_{71}BM$ aggregate structures from the active layer matrix, rather than the pieces stripped from ITO substrates in the traditional TEM measurement, the $PC_{71}BM$ aggregate morphology induced by the additives could be clearly shown. The results suggest the mechanism of the performance enhancement of the PSC devices with the different binary additive treatments.

Received: August 9, 2014
Published: November 11, 2014

EXPERIMENTAL SECTION

Preparation and Characterization of the $PC_{71}BM$ Aggregate Morphology. PBDTTT-C-T and $PC_{71}BM$ (see Figure 1a) was purchased from Solarmer and Nano-C,

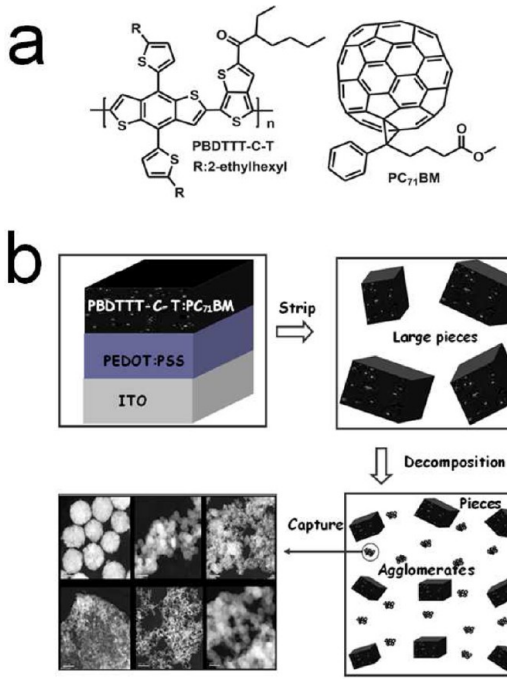

Figure 1. (a) Molecular structures of PBDTTT-C-T and $PC_{71}BM$. (b) Schematic depiction of preparing and characterizing the aggregate $PC_{71}BM$ structures.

respectively. The schematic depiction of preparing and characterizing the $PC_{71}BM$ aggregate structures is displayed in Figure 1b. The ITO glass with a sheet resistance of 10 Ω s q^{-1} was cleaned by sequential ultrasonic treatment in detergent, deionized water, acetone, and isopropanol and then treated in an ultraviolet-ozone chamber for 15 min. Then a PEDOT:PSS buffer layer was spin-coated on the ITO substrate with a speed of 2000 rpm. The blend solution of PBDTTT-C-T:$PC_{71}BM$ (1:1.5 w/w, 12.5 mg/mL for PBDTTT-C-T) in dichlorobenzene (DCB) was spin-coated on top of the PEDOT:PSS at 1200 rpm with the spin-coating time of 60 s. The samples were immersed in deionized water. After 10 min, ultrasonic processing with a 100 W power, large pieces were commonly ultrasonic stripped from ITO substrates in deionized water. With subsequent ultrasonic treatment for 10 min, the pieces will decompose to small pieces and $PC_{71}BM$ aggregate structures, which floated in water and around the edges of the small pieces. The aggregate structures were obtained via washing out the polymer from the active layers by 20 min ultrasonic treatment in deionized water. After salvaging with copper nets covered by a carbon film several times, and then seeking around the edges of the smaller pieces and in the region of the carbon film, we capture the $PC_{71}BM$ aggregate structures. Finally, the aggregate structures are distinctly characterized by TEM.

Fabrication and Characterization of the PSC Devices. The PSC devices with a structure of ITO/PEDOT:PSS/PBDTTT-C-T[15]:$PC_{71}BM$/Ca/Al were fabricated. The processes of cleaning ITO and preparing PEDOT:PSS and PBDTTT-C-T:$PC_{71}BM$ were in accord with the above processes. Then, the negative electrode of Ca (~20 nm)/Al (~100 nm) was thermally evaporated on the active layer under a shadow mask in a base pressure of about 10^{-4} Pa. The current density−voltage (J−V) curves of the cells were measured with a computer-controlled Keithley 236 Source Measure Unit under the illumination of AM1.5G, 100 mW cm^{-2} using a xenon-lamp-based solar simulator (from Newport Co., Ltd.). The external quantum efficiency (EQE) was conducted on a Stanford Research Systems DSP lock-in amplifier (SR830) linked with a 500 W xenon lamp. The morphologies of the $PC_{71}BM$ aggregate structures and the active layers were investigated by TEM (TECNAI G20, FEI).

RESULTS AND DISCUSSION

Optimization of the Performance of the PSC Devices by Binary Additives. We carried out the optimization of the PSC devices based on PBDTTT-C-T:$PC_{71}BM$ with the single additives and the binary additives of different vol. ratios. Figure 2a shows the J−V curves of the devices, under the illumination

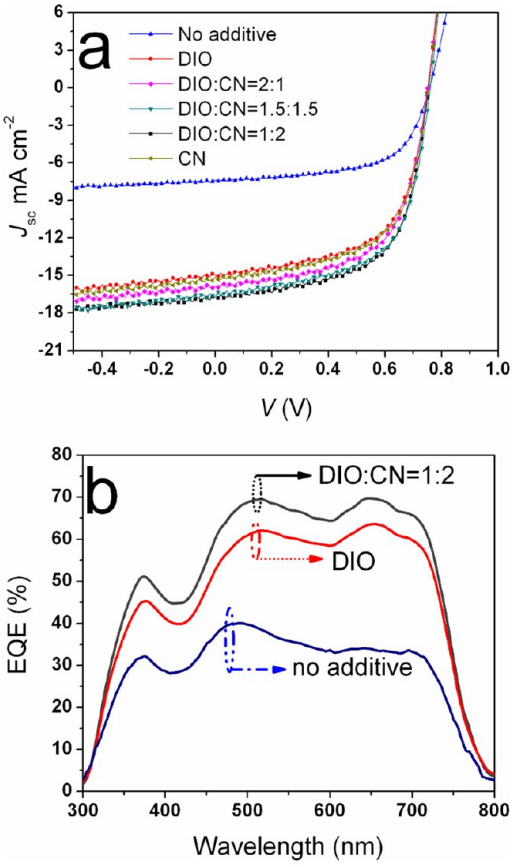

Figure 2. (a) J−V characteristics and (b) EQE spectra of the PBDTTT-C-T:$PC_{71}BM$ PSC devices.

of AM 1.5G, 100 mW cm^{-2}. Table 1 summarizes the performance parameters of the devices. For all the devices, V_{oc} is almost independent with the additives treatment, which is in the range of 0.75−0.76 V. The fill factor (FF) of the devices with the different additive treatment just changes a little, in the range of 60.9~62.7%. However, the J_{SC} of the PSC devices changes significantly with the treatment of different DIO/CN vol. ratios of 3:0, 2:1, 1.5:1.5, 1:2, and 0:3. For the devices without additive treatment, the J_{SC} is only 7.39 mA cm^{-2}. Using

dx.doi.org/10.1021/ph500295p | ACS Photonics 2014, 1, 1278−1284

Table 1. Summary of the Performance of the PBDTTT-C-T:$PC_{71}BM$ Devices without Additive Treatment and with the Additive Treatment

additives DIO/CN	V_{OC} (V)	J_{SC} (mA cm^{-2})	FF (%)	PCE (%)	size (nm)	μ_e (cm^2/V s)
none	0.76	7.39	61.2	3.44	160	2.75×10^{-4}
3:0	0.75	15.02	60.9	6.86	70	1.04×10^{-3}
2:1	0.75	15.83	61.4	7.29		1.33×10^{-3}
1.5:1.5	0.76	16.65	61.3	7.76	13	1.71×10^{-3}
1:2	0.75	16.81	62.7	7.91	9	2.10×10^{-3}
0:3	0.75	15.13	61.5	6.98	55	1.14×10^{-3}

a 3% vol. DIO additive leads to a noticeable increase in J_{SC} to 15.02 mA cm^{-2}. Whereas with the treatment of the 1:2 binary additives, the highest J_{SC} and PCE reaches 16.81 mA cm^{-2} and 7.91%, respectively. Figure 2b shows the EQE plots of the three devices with different treatment: without additive treatment, with the 3% DIO treatment, and with the 1:2 DIO/CN binary additive treatment. The EQE results agree very well with the J_{SC} values mentioned above. The EQE reaches ~70% at 515 and 645 nm for the PSC with the 1:2 binary additive treatment, which corresponds to the highest J_{SC} of 16.81 mA cm^{-2}. The EQE values at 515 nm and at 645 nm are reduced to ~62 and ~64%, respectively, for the PSC with the 3% DIO additive treatment, whereas the PSC without any additive treatment shows the lowest EQE value of ~40%.

PBDTTT-C-T:$PC_{71}BM$ Film Morphology. For understanding the effect of the additives treatment on the film morphology and the photovoltaic performance of the PSC devices, we investigated the morphology evolution of the active layers of the devices. The film morphology was illustrated by the traditional TEM characterization with stripping the active layer from PEDOT:PSS/ITO substrates. Figure 3 shows the TEM images of the PBDTTT-C-T:$PC_{71}BM$ films processed without additive treatment and with the additive treatments: a, no additive; b, 3:0; c, 2:1; d, 1.5:1.5; e, 1:2; f, 0:3. It should be noted that the white and black domains in the TEM images represent $PC_{71}BM$-rich domains and polymer-rich domains, respectively. In Figure 3a,b, the active layers without additive treatment and with the DIO treatment were orderly embedded with many large $PC_{71}BM$-rich domains. The size of the $PC_{71}BM$-rich domains without any additive treatment is 1.5–2.5-fold bigger than that of the $PC_{71}BM$-rich domains with the DIO treatment. Moreover, the $PC_{71}BM$-rich domains in the active layer with the DIO treatment became closely aligned, suggesting that the DIO additive treatment restrained the large-domain aggregate of $PC_{71}BM$ molecules. However, both the TEM images cannot probe the lateral morphology of $PC_{71}BM$ domains in the active layers yet. Afterward, compared to that in Figure 3a, less $PC_{71}BM$-rich domains were found in Figure 3c–f, suggesting a better phase segregated morphology. Whereas Figure 3e shows well-distributed and homogeneous domains over the entire area of the TEM images. Little large-domain aggregates were found in Figure 3e. According to the above results, there is still limited information regarding the film and the aggregate morphology. Hence, the traditional TEM characterization does not meet the requirements of a distinct and fine characterization of the $PC_{71}BM$ aggregate morphology.

$PC_{71}BM$ Aggregate Morphology. In order to get distinct morphologies of the $PC_{71}BM$ aggregates, a novel TEM measurement was employed by washing out the polymer donor from the active layers. The morphology results are presented in Figures 4–9.

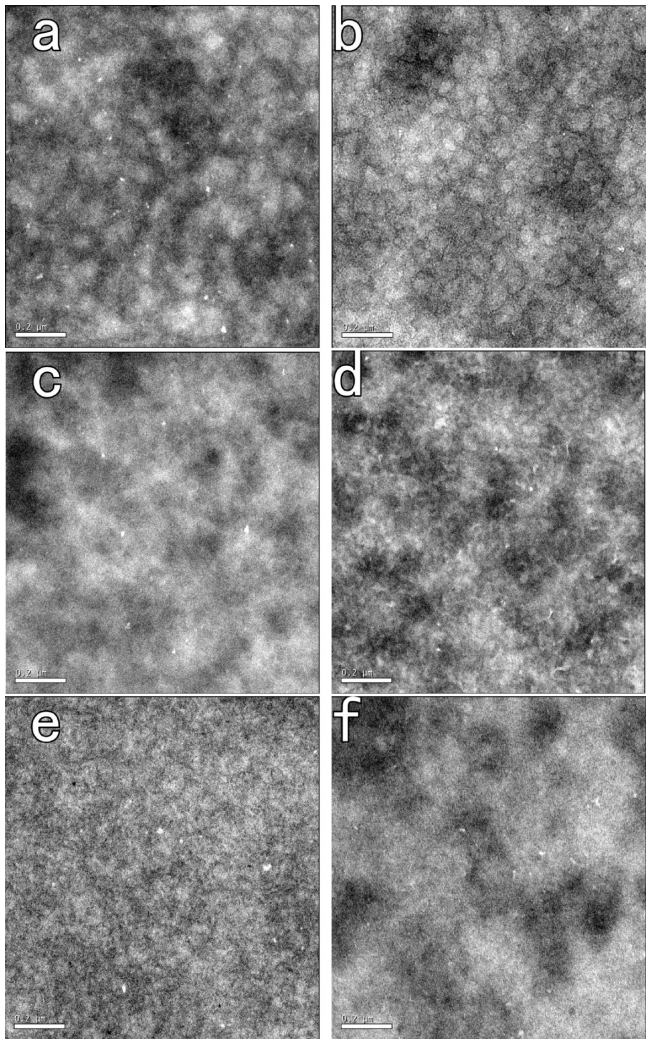

Figure 3. TEM images of PBDTTT-C-T:$PC_{71}BM$ active layers: (a) no additive, (b) DIO, (c) 2:1 DIO/CN, (d) 1.5:1.5, (e) 1:2, and (f) CN. Scale bars: 0.2 μm.

Figure 4 shows the morphology of $PC_{71}BM$ aggregate structure without additive treatment. In Figure 4a,c, the black region represents the carbon film, the gray region represents the active layer, and the white region represents $PC_{71}BM$ domain. It shows many large $PC_{71}BM$ spheres on the carbon film and on the active layer. The TEM images in Figure 4a,c were obtained in two samples, implying a good stability in the morphology of the $PC_{71}BM$ spheres. Figure 4b,d is the amplified image of Figure 4a and c, respectively. In Figure 4d, it shows a convincing evidence that the larger spheres are composed of much smaller $PC_{71}BM$ nanoparticles, which symmetrically assemble on the coarse surfaces of the $PC_{71}BM$ spheres. Attributed to the massive $PC_{71}BM$ spheres were embedded and less individual aggregate with much smaller sizes were found in the active layer, the $PC_{71}BM$ spheres are the major existence of $PC_{71}BM$ molecules in the whole active layers.

Figure 5 shows the morphology of $PC_{71}BM$ aggregate structure with the 3% vol. DIO additive treatment. Figure 5a,d displays the $PC_{71}BM$ aggregate structure at two places in the sample. It shows a penetrating $PC_{71}BM$ network, which is

dx.doi.org/10.1021/ph500295p | ACS Photonics 2014, 1, 1278–1284

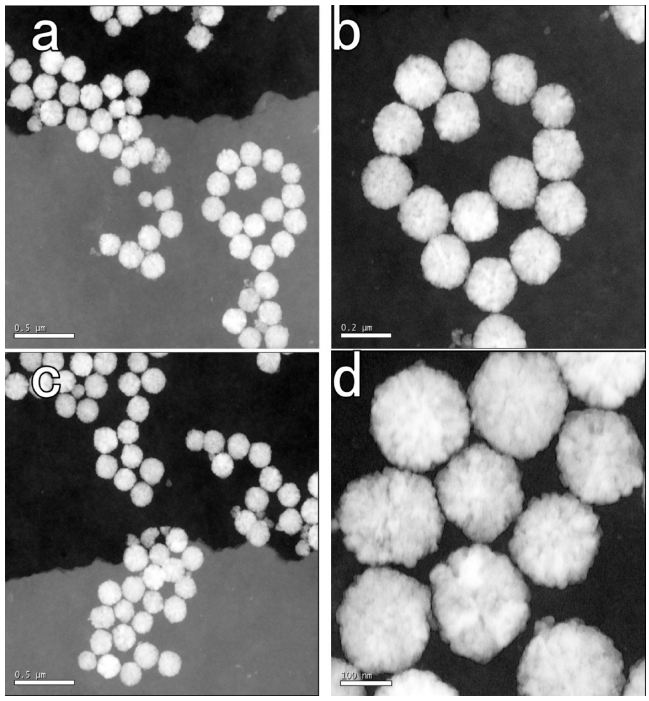

Figure 4. TEM images of $PC_{71}BM$ aggregate structure without additive treatment. Scale bars: (a, c) 0.5 μm, (b) 0.2 μm, and (d) 100 nm.

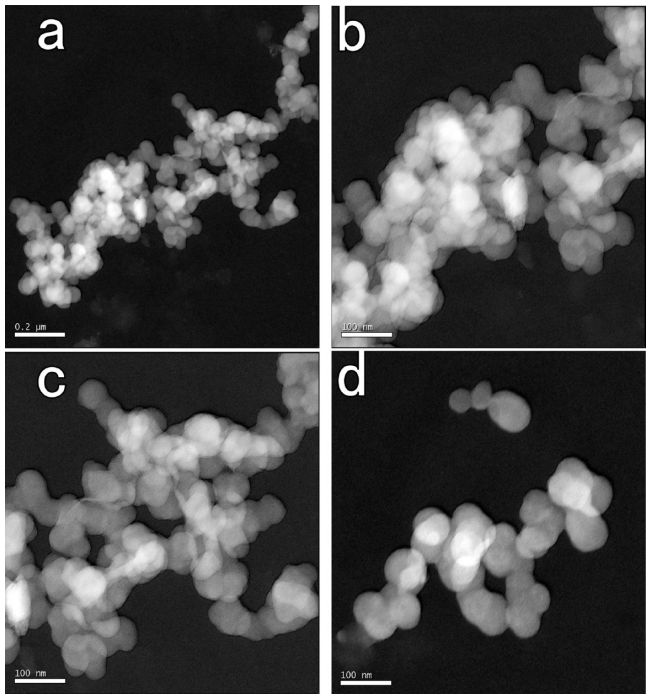

Figure 5. TEM images of $PC_{71}BM$ aggregate structure with the 3% DIO additive treatment. Scale bars: (a) 0.2 μm, (b–d) 100 nm.

composed of $PC_{71}BM$ particles with a major size of 60–80 nm, and the particles are much smaller than the $PC_{71}BM$ spheres without additive treatment. The results indicate a significant reduction in the size of the aggregate $PC_{71}BM$ particles by using the 3% DIO additive treatment. Figure 5b and c are the amplified images of Figure 5a. The aggregate particles of 60–80 nm overlapped each other to form continuous pathways with many contact points/interfaces. Moreover, the surface of the structure is much smoother than that of the large spheres without additive treatment. The relationship between the contact points/interfaces, the aggregate surfaces, and the charge-carrier transport property will be required to study in the future.

Figure 6 shows the morphology of $PC_{71}BM$ aggregate structure with the treatment of the DIO/CN vol. ratio of 2:1.

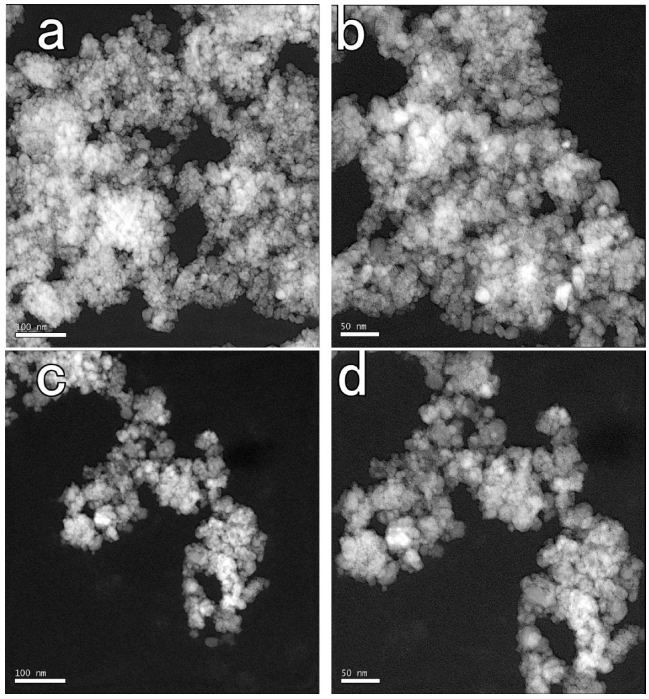

Figure 6. TEM images of $PC_{71}BM$ aggregate structure with the 2:1 binary additive treatment. Scale bars: (a, c) 100 nm, (b, d) 50 nm.

Such a morphology was achieved in two samples, as shown in Figure 6a,b and c,d, respectively. It shows a disorganized aggregate structure, similar to "white clouds in the sky". Compared to the $PC_{71}BM$ aggregate structure with DIO treatment, it displays coarser pathways with smaller aggregates. Moreover, in the images, the color is more white, the $PC_{71}BM$ aggregates were larger, and thus, polymer molecules will, with difficulty permeate the white $PC_{71}BM$ domains, which is unfavorable to phase segregation. However, compared to the $PC_{71}BM$ structure with DIO treatment, the $PC_{71}BM$ structure with 2:1 additive treatment exhibits finer fullerene pathways and larger interfacial areas for exciton dissociation and charge-carrier transport.

Figure 7a shows the morphology of $PC_{71}BM$ aggregate structure with the 1.5:1.5 binary additive treatment. It presents an interconnected and uniformly dispersed $PC_{71}BM$ network. The $PC_{71}BM$ particles in the white and gray domains exhibit a major size of 10–16 nm. Figure 7b is the amplified images of Figure 7c. In the distinct image, the small $PC_{71}BM$ particles are stacked well without large-domain aggregation. Moreover, it exhibits quantities of fine and well-ordered pathways for electron transport in the aggregate structure, as well as coarse surfaces for exciton dissociation. The quality of the $PC_{71}BM$ penetrating network is checked to be better in the above TEM images, which is favorable to obtain large interfacial areas and good interpenetrating pathways for a higher J_{SC}.

dx.doi.org/10.1021/ph500295p | ACS Photonics 2014, 1, 1278–1284

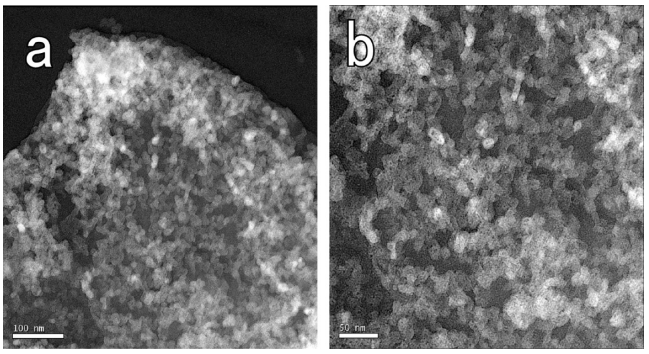

Figure 7. TEM images of $PC_{71}BM$ aggregate structure with the 1.5:1.5 binary additive treatment. Scale bars: (a) 100 nm, (b) 50 nm.

Figure 8a shows the morphology of $PC_{71}BM$ aggregate structure with the 1:2 binary additive treatment. Compared to

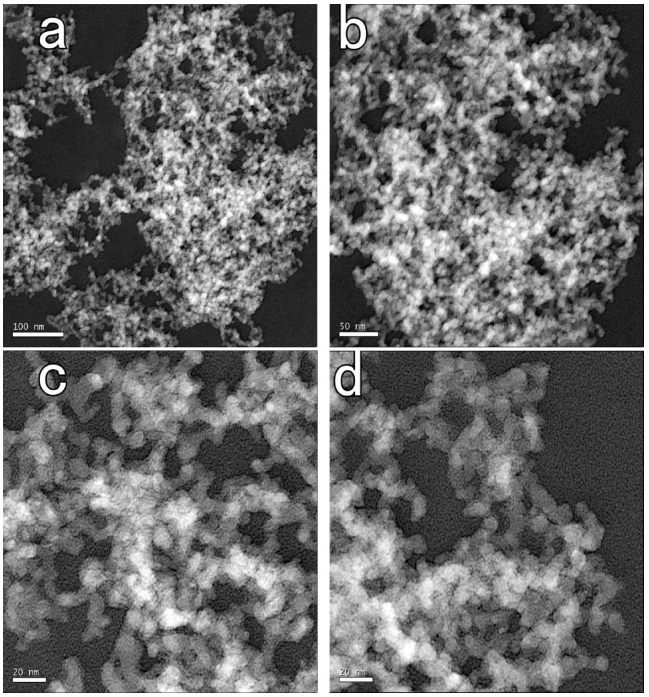

Figure 8. TEM images of $PC_{71}BM$ aggregate structure with the 1:2 binary additive treatment. Scale bars: (a) 100, (b) 50, and (c, d) 20 nm.

the particles with the 1.5:1.5 additive treatment, it shows smaller particles with a major size of 8−10 nm, leading to the most sufficient interfacial contact of polymer/$PC_{71}BM$. It is worth noting that the 8−10 nm sizes of $PC_{71}BM$ particles provides an direct evidence of the desired length scale, which was speculated to be an ideal value for exciton dissociation.[16−18] Moreover, the 1:2 binary additives profoundly alters the stack way of the $PC_{71}BM$ particles. The film cast from 2:1 binary additives shows a collapsing and loose $PC_{71}BM$ aggregate structure, inducing a relatively poor phase segregation, whereas both the films with the 1.5:1.5 and the 1:2 binary additives show a finely dispersed and ordered distributed domain (white and gray). After the 1.5:1.5 binary additive treatment, $PC_{71}BM$ particles exhibit a tendency to stand in the structure, and upon the 1:2 binary additive treatment, most $PC_{71}BM$ particles are interlocked rigidly each other to form fine and close-packed pathways, implying the largest donor/acceptor interface areas and, hence, inducing more efficient exciton dissociation and charge-carrier transport for the best PSC devices.

Figure 9 shows the morphology of $PC_{71}BM$ aggregate structure with the 3.0% CN additive treatment. A noticeable

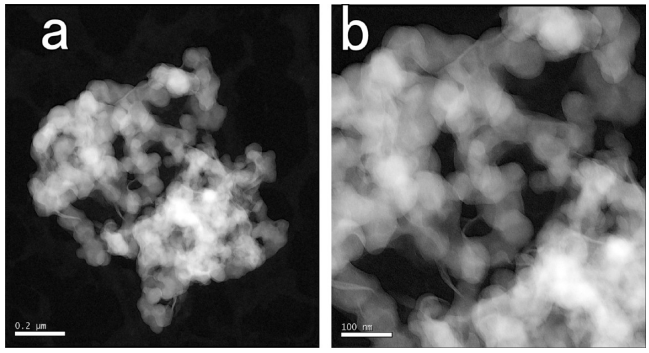

Figure 9. TEM images of $PC_{71}BM$ aggregate structure with the 3% CN additive treatment: (a) 0.2 μm and (b) 100 nm.

increase in the major sizes of 40−80 nm was observed for the $PC_{71}BM$ particles. And the $PC_{71}BM$ particles were stacked together to form a smooth pathway. The internal morphology induced by the CN is similar to that induced by the DIO, suggesting a general characteristic of $PC_{71}BM$ aggregate regulated by the single additives.

To clearly compare all the $PC_{71}BM$ aggregate structures with different additive treatments, we select and summarize the TEM images with the same scale bar of 100 nm, as shown in Figure 10. It distinctly presents the variation of all the $PC_{71}BM$ aggregate morphology.

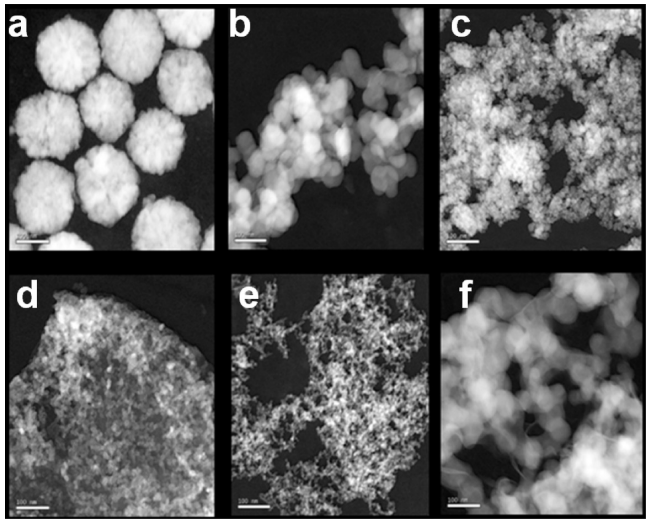

Figure 10. TEM images of $PC_{71}BM$ aggregate structures with different additive treatments: (a) no additive, (b) DIO, (c) 2:1 DIO/CN, (d) 1.5:1.5, (e) 1:2, (f) CN. Scale bars: 100 nm.

Correlation between the $PC_{71}BM$ Aggregate Size and the Device Performance. Our results presents a significant link between the $PC_{71}BM$ aggregate structures and the performance of the PSC devices. As is well-known, $PC_{71}BM$ molecules can be dissolved in DIO and CN, whereas polymer molecules cannot.[19] The boiling point of DCB, DIO, and CN is

dx.doi.org/10.1021/ph500295p | ACS Photonics 2014, 1, 1278−1284

131.7, 167, and 263 °C, respectively. In spin-coating the blend solution process, PBDTTT-C-T molecules were precipitated from DCB, whereas $PC_{71}BM$ molecules were subsequently precipitated from DCB, DIO, and CN. The precipitating process of acceptors can be determined by the content of DIO additive (0.25−1%,[10] 2−7%,[20,21] and 10%[22]), the ternary solvents of DCB/chloroform/DIO (ratio: 79:19:5%),[23] the ratios of DIO/CN additives (1:4%, 3:4%, 1:10%, and 3:10%), the solvent selection of CB/DCB (CB is much better than DCB in the previous work),[22] and so on. Here, the $PC_{71}BM$ aggregate structures were optimized by slightly tuning the binary additive ratios. The histogram of the particle sizes are shown in Figure 11. It clearly presents the dimension

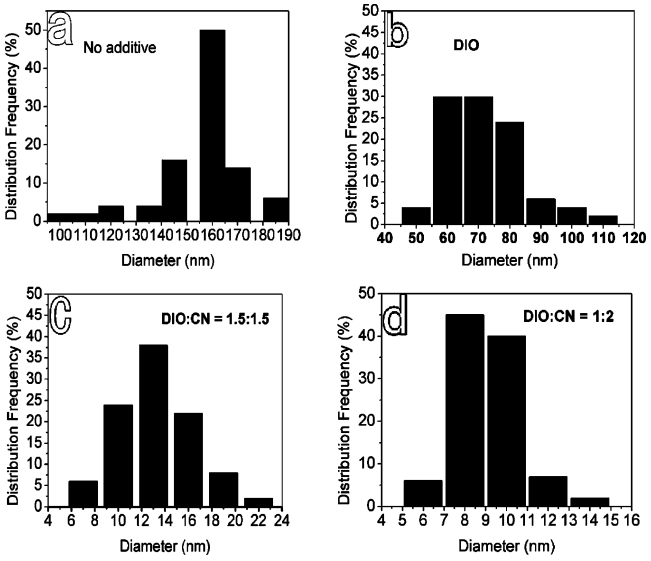

Figure 11. Dimension distribution of $PC_{71}BM$ particles without additive treatment (a) and with additive treatment of (b) DIO, (c) 1.5:1.5 binary additives, and (d) 1:2 binary additives.

distribution of every $PC_{71}BM$ particle in the corresponding $PC_{71}BM$ aggregate structure without additive treatment (a), and with DIO (b), 1.5:1.5 (c), and 1:2 (d) binary additive treatment, respectively. According to the qualitative analysis of $PC_{71}BM$ aggregate morphology, the sizes of the major aggregate particles (>80%) are changed from 145 to 170 nm (a), 60−80 nm (b), 10−16 nm (c), and 8−10 nm (d), respectively. Figure 12a displays the plots of J_{SC} and the PCE as a function of average $PC_{71}BM$ aggregate sizes according to the TEM images (~160 nm for no additive, ~70 nm for DIO, ~55 nm for CN, ~13 nm for 1.5:1.5 additives, and ~9 nm for 1:2 additives). It indicates a key role of DIO/CN to control the $PC_{71}BM$ particle sizes. The optimized 1:2 binary additives induce the best morphology of fine, dense and packed-well pathway for the highest J_{SC} and PCE.

Moreover, to precisely assess the effect of the $PC_{71}BM$ aggregate morphology on the electron mobility (μ_e), we have carefully examined the electron mobility as a function of the different additive treatments by the space charge limited current (SCLC) model using Theott−Gurney square law. Figure 12b displays the $J_D^{0.5}$-V curves of the Al (100 nm)/PBDTTT-C-T:$PC_{71}BM$/Al (100 nm) electron-only devices as a function of the different additive conditions. Clear correlations between the particle sizes and the μ_e values are presented in Figure 12c. It shows that the μ_e value increases with the decrease of the size of

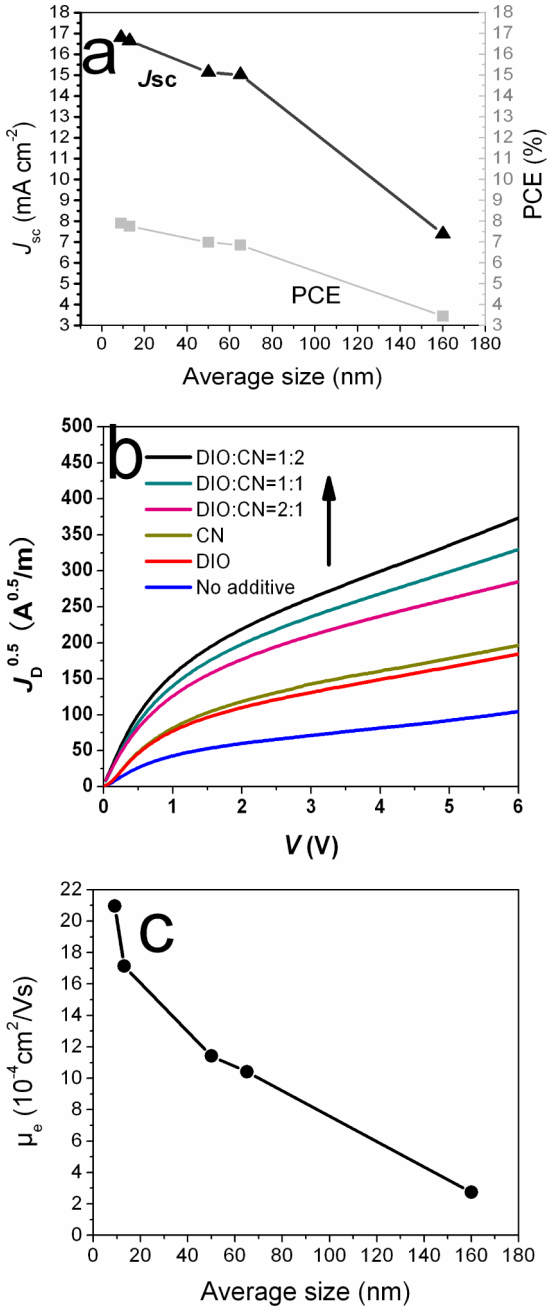

Figure 12. (a) Curve of J_{SC} and PCE as a function of particle sizes, (b) the $J_D^{0.5}$−V curve of the electron-only devices, and (c) the curve of μ_e as a function of particle sizes.

the $PC_{71}BM$ particles. The μ_e with the1:2 binary additives is about double that of single additive and is 7.6 times that without additives.

The results indicate that a good aggregate structure with smaller $PC_{71}BM$ particles, which can induce larger donor/acceptor interfaces and better penetrating pathways, are in favor of exciton separation and charge-carrier transport for higher μ_e, and thus, leading to an enhancement in J_{SC} and PCE.[24]

CONCLUSION

The power conversion efficiency of the PBDTTT-C-T:$PC_{71}BM$ PSC devices was significantly improved from 3.44% for the PSC without additive to 7.91% with the binary additive of 1% DIO and 2% CN, by precisely regulating the vol. ratio of binary

dx.doi.org/10.1021/ph500295p | ACS Photonics 2014, 1, 1278−1284

processing additives of DIO and CN. In our TEM measurement, the morphologies of the $PC_{71}BM$ aggregate structures were clearly demonstrated for all the active layer in the PSC devices. It presents connected $PC_{71}BM$ spheres with a major size (diameter) of 160 ± 15 nm in the active layer matrix without additive treatment, which were composed of much smaller $PC_{71}BM$ particles with a size of below 20 nm. With the 3% DIO treatment, continuous and interlaced pathways with smaller aggregate $PC_{71}BM$ particles (~70 nm) were observed. With the 1:2 DIO/CN binary additive treatment, the $PC_{71}BM$ aggregate exhibit fine, orderly stacked and penetrating networks with particles of a size of 8−10 nm, which corresponds to the best photovoltaic performance of the PSC. Correlation of $PC_{71}BM$ aggregate morphology and photovoltaic performance of PSC devices were studied. It presents that highly efficient PSC devices were achieved with a good $PC_{71}BM$ aggregate structure of small particles, and fine, dense, and well-packed pathways. Our work provides a new way for distinctly characterizing and regulating the lateral morphologies of the $PC_{71}BM$ aggregate structures for highly efficient PSC devices.

AUTHOR INFORMATION

Corresponding Authors

*E-mail: fanxi.2008@163.com.

*E-mail: nanoguy@126.com.

Notes

The authors declare no competing financial interest.

ACKNOWLEDGMENTS

This work is supported in part by the National Nature Science Foundation of China (No. 51372075) and Research Fund for the Doctoral Program of Higher Education of China (RFDP, No. 20124208110006).

REFERENCES

(1) Jonathon, W. K.; Aaron, P. R. E.; Michael, E. M. Nanoparticle Aggregate in Polymer-Based Solar Cells. *Phys. Rev. Lett.* **2010**, *105*, 168701.

(2) Li, G.; Shrotriya, V.; Huang, J. S.; Yao, Y.; Moriarty, T.; Emery, K.; Yang, Y. High-Efficiency Solution Processable Polymer Photovoltaic Cells by Self-Organization of Polymer Blends. *Nat. Mater.* **2005**, *4*, 864−868.

(3) Park, S. H.; Roy, A.; Beaupre, S.; Cho, S.; Coates, N.; Moon, J.-S.; Moses, D.; Leclerc, M.; Lee, K.; Heeger, A. J. Bulk Hetero-Junction Solar Cells with Internal Quantum Efficiency Approaching 100%. *Nat. Photonics* **2009**, *3*, 297−302.

(4) Li, Y. F. Molecular Design of Photovoltaic Materials for Polymer Solar Cells: Towards Suitable Electronic Energy Levels and Broad Absorption. *Acc. Chem. Res.* **2012**, *45*, 723−733.

(5) Bull, T. A.; Pingree, L. S. C.; Jenekhe, S. A.; Ginger, David. S.; Luscombe, C. K. The Role of Mesoscopic PCBM Crystallites in Solvent Vapor Annealed Copolymer Solar Cells. *ACS Nano* **2009**, *3*, 627−636.

(6) Xin, H.; Reid, O. G.; Ren, G. Q.; Kim, F. S.; Ginger, D. S.; Jenekhe, S. A. Polymer Nanowire/Fullerene Bulk Hetero-junction Solar Cells: How Nanostructure Determines Photovoltaic Properties. *ACS Nano* **2010**, *4*, 1861−1872.

(7) Xin, H.; Guo, X. G.; Ren, G. Q.; Watson, M. D.; Jenekhe, S. A. Efficient Phthalimide Copolymer-Based Bulk Hetero-Junction Solar Cells: How the Processing Additive Influences Nanoscale Morphology and Photovoltaic Properties. *Adv. Energy Mater.* **2012**, *2*, 575−582.

(8) Warnan, J.; Labban, A. E.; Cabanetos, C.; Hoke, E. T.; Shukla, P. K.; Risko, C.; Bredas, J.-L.; McGehee, M. D.; Beaujuge, P. M. Ring Substituents Mediate the Morphology of PBDTTPD-PCBM Bulk Hetero-Junction Solar Cells. *Chem. Mater.* **2014**, *26*, 2299−2306.

(9) Wu, W. R.; Jeng, U.; Su, C. J.; Wei, K. H.; Su, M. S.; Chiu, M. Y.; Chen, C. Y.; Su, W. B.; Su, C. H.; Su, A. C. Competition between Fullerene Aggregation and Poly(3-hexylthiophene) Crystallization upon Annealing of Bulk Hetero-Junction Solar Cells. *ACS Nano* **2011**, *5*, 6233−6243.

(10) Sun, Y. M.; Welch, G. C.; Leong, W. L.; Takacs, C. J.; Bazan, G. C.; Heeger, A. J. Solution-Processed Small-Molecule Solar Cells with 6.7% Efficiency. *Nat. Mater.* **2012**, *11*, 44−48.

(11) Chen, W.; Nikiforov, M. P.; Darling, S. B. Morphology Characterization in Organic and Hybrid Solar Cells. *Energy Environ. Sci.* **2012**, *5*, 8045−8074.

(12) Yip, H.-L.; Jen, A. K. Y. Recent Advances in Solution-Processed Interface Materials for Efficient and Stable Polymer Solar Cells. *Energy Environ. Sci.* **2012**, *5*, 5994−6011.

(13) Moule', A. J.; Meerholz, K. Morphology Control in Solution-Processed Bulk Hetero-Junction Solar Cell Mixtures. *Adv. Funct. Mater.* **2009**, *19*, 3028−3036.

(14) Andersson, B. V.; Herland, A.; Masich, S.; Inganas, O. Imaging of the 3-D Nanostructure of A Polymer Solar Cell by Electron Tomography. *Nano Lett.* **2009**, *9*, 853−855.

(15) Huo, L. J.; Zhang, S. Q.; Guo, X.; Xu, F.; Li, Y. F.; Hou, J. H. Replacing Alkoxy Groups with Alkylthienyl Groups: A Feasible Approach To Improve the Properties of Photovoltaic Polymers. *Angew. Chem., Int. Ed.* **2011**, *50*, 9697−9702.

(16) Ma, W.; Yang, C.; Gong, X.; Lee, K.; Heeger, A. J. Thermally Stable, Efficient Polymer Solar Cells with Nanoscale Control of the Interpenetrating Network Morphology. *Adv. Funct. Mater.* **2005**, *15*, 1617−1622.

(17) Fan, X.; Fang, G. J.; Qin, P. L.; Cheng, F.; Zhao, X. Z. Rapid Phase Segregation of P3HT:PCBM Composites by Thermal Annealing for High-Performance Bulk-Hetero-Junction Solar Cells. *Appl. Phys. A: Mater. Sci. Process.* **2011**, *105*, 1003−1009.

(18) Fan, X.; Cui, C. H.; Fang, G. J.; Wang, J.; Li, S.; Cheng, F.; Long, H.; Li, Y. Efficient Polymer Solar Cells Based on Poly(3-hexylthiophene):Indene-C_{70} Bisadduct with a MoO_3 Buffer Layer. *Adv. Funct. Mater.* **2012**, *22*, 585−590.

(19) Lee, J. K.; Ma, W. L.; Brabec, C. J.; Yuen, J.; Moon, J. S.; Kim, J. Y.; Lee, K.; Bazan, G. C.; Heeger, A. J. Processing Additives for Improved Efficiency from Bulk Hetero-Junction Solar Cells. *J. Am. Chem. Soc.* **2008**, *130*, 3619−3623.

(20) Kim, Y.; Yeom, H. R.; Kim, J. Y.; Yang, C. High-efficiency Polymer Solar Cells with A Cost-effective Quinoxaline Polymer through Nanoscale Morphology Control Induced by Practical Processing Additives. *Energy Environ. Sci.* **2013**, *6*, 1909−1916.

(21) Guo, X.; Cui, C. H.; Zhang, M. J.; Huo, L. J.; Huang, Y.; Hou, J. H.; Li, Y. High Efficiency Polymer Solar Cells Based on Poly(3-hexylthiophene)/Indene-C-70 Bisadduct with Solvent Additive. *Energy Environ. Sci.* **2012**, *5*, 7943−7949.

(22) Réda, B.; Lu, J. P.; Beaupré, S.; Leclerc, M.; Tao, Y. Control of The Active Layer Nanomorphology by Using Co-Additives towards High-Performance Bulk Hetero-Junction Solar Cells. *Org. Electron.* **2012**, *13*, 1736−1741.

(23) Ye, L.; Zhang, S. Q.; Ma, W.; Fan, B. H.; Guo, X.; Huang, Y.; Ade, H.; Hou, J. H. From Binary to Ternary Solvent: Morphology Fine-Tuning of D/A Blends in PDPP3T-Based Polymer Solar Cells. *Adv. Mater.* **2012**, *24*, 6335−6341.

(24) Pandey, A. K.; Aljada, M.; Pivrikas, A.; Velusamy, M.; Burn, P. L.; Meredith, P.; Namdas, E. B. Dynamics of Charge Generation and Transport in Polymer-Blends Elucidated Using a PhotoFET Architecture. *ACS Photonics* **2014**, *1*, 114−120.